Effect of nickel on the high-pressure phases in FeH

Helene Piet,[1,*] Andrew V. G. Chizmeshya,[2] Bin Chen,[3] Stella Chariton,[4]
Eran Greenberg,[4] Vitali B. Prakapenka,[4] and Sang-Heon Shim[1,†]
[1]*School of Earth and Space Exploration, Arizona State University, Tempe, Arizona, USA*
[2]*School of Molecular Sciences, Arizona State University, Tempe, Arizona, USA*
[3]*Hawaii Institute of Geophysics and Planetology, University of Hawaii at Manoa, Honolulu, Hawaii, USA*
[4]*Center for Advanced Radiation Sources, University of Chicago, Chicago, Illinois, USA*

(Received 6 July 2021; revised 25 October 2021; accepted 14 December 2021; published 21 December 2021)

Hydrogen-rich metal alloys and compounds have drawn interest from planetary geophysics and condensed matter physics communities because of their potential for deep hydrogen storage in planets and high-temperature superconductivity. We find that a small amount of Ni can alter the phase behavior in the FeH alloy system. Ni can stabilize the double hexagonal close-packed (dhcp) structure in FeH up to the liquidus at 33 GPa, which is in contrast with the stability of the face-centered cubic (fcc) structure in Ni-free FeH at the same conditions. Above 60 GPa, Ni suppresses the stability of the tetragonal FeH_2 phase but stabilizes fcc FeH at higher temperatures. At the same pressure range, we find tetragonal FeH_2 and cubic FeH_3 to be stable at temperatures above 2500 K without Ni. Therefore, in planetary interiors, Ni will expand the stability field of dense close-packed structures in the FeH system. If the Ni content is low, then FeH_2 and FeH_3 can play an important role in the cores of hydrogen-rich planets. Also, our study demonstrates that a secondary alloying component can severely impact the high-pressure stability of polyhydrides.

DOI: 10.1103/PhysRevB.104.224106

I. INTRODUCTION

Iron (Fe) and nickel (Ni) are naturally abundant 3*d* transition metals and dominant elements in planetary cores [1]. Both Fe and Ni have also been shown to alloy with hydrogen at high pressures relevant for planetary interiors, opening up a possibility for a large storage of hydrogen in the core as a light element [2,3]. In fact, recent partitioning experiments have shown that a large amount of H (0.3–0.6 wt. %) could have been incorporated into the core during early Earth differentiation [4]. Recent InSight mission data analysis found a much greater radius of the core than previously estimated, requiring a large amount of light elements in the martian core [5]. To explain the low density of the martian core, hydrogen up to 2 wt. % was considered along with carbon and sulfur as light elements, which corresponds to a molar H/Fe ratio of approximately 1. In these efforts, it is essential to know the impact of Ni which is an important alloying component for the planetary cores (∼5% for the Earth's core). Important differences have been identified between the FeH and NiH systems [6–9]. For example, face-centered cubic (fcc) phase appears to be more stable in NiH_x, whereas double hexagonal close-packed (dhcp) structure is more stable in FeH_x at low temperatures and high pressures [9]. Note that the structure types discussed in the literature for FeH and NiH alloys, such as fcc, dhcp, and hcp (hexagonal close-packed) structures, describe the structures of the Fe (or Ni) sublattices. H atoms enter the interstitial sites of the Fe (or Ni) sublattice. FeH_x begins to form polyhydrides with direct H-to-H bonding at pressures above ∼60 GPa, such as tetragonal FeH_2, cubic FeH_3, and tetragonal FeH_5 [7,10], but these structures have not yet been found in NiH [8,9]. In addition, H-rich polyhydrides found in FeH were all synthesized at temperatures lower than ∼1500 K and therefore uncertainty remains regarding their relevance for the planetary cores.

In condensed matter physics, record-high critical temperatures have been recently reported in some hydrogen-rich materials, H_3S (T_c = 203 K at 150 GPa) [11] and LaH_{10} (T_c = 260 K at 190 GPa) [12]. Polyhydrides have also been found in the FeH system at high pressures [7,10]. Whether any of these polyhydride phases found in FeH could have high temperature superconductivity is under debate [10,13]. A recent theoretical study found that doping of FeH compounds with Ni could alter the properties [13]. More fundamentally, it would be beneficial to understand which factors can control the amount of hydrogen in metal-hydrogen alloys and whether changing alloy components can affect the stable *P-T* conditions of crystal structures in this important system.

In this paper we report experimental results on the phase behaviors of the FeH and (Fe,Ni)H systems at high pressures and high temperatures. In the experiments, high pressure-temperature conditions were achieved in the double-sided laser heating diamond-anvil cell. Synchrotron x-ray diffraction patterns were measured before, during, and after laser heating for phase identification. The data sets enable us to understand the effect of Ni on the phase behaviors of FeH system.

II. METHODS

Pure metallic iron was obtained from reagent grade powder from Alfa Aesar. We synthesized an FeNi alloy with

*helene.m.piet@gmail.com
†shdshim@asu.edu

TABLE I. Experimental runs. P: pressure measured before heating and T: temperature range during heating. For example, during a heating cycle in run 231, the sample experienced a range of temperatures between 1690 and 2179 K. For the runs with single temperatures, a fixed temperature was maintained during heating. Temperature uncertainties [$\sigma(T)$] were determined from the difference between measured temperatures on both sides of the LHDAC. In the case where the difference was below 150 K, we assigned 150 K. The last column (Texture) provides information on possible melting based on visual observations after laser heating at high pressures, subliq.: subliquidus data points inferred from no clear eye-shaped structure; and liq.: liquidus data points for the higher temperatures recorded during the run inferred from an eye-shaped structure. For run 203, the cell failed during heating and therefore we do not have visual observation after the laser heating. The "Phases" column includes the phases observed in XRD patterns, dhcp: dhcp FeH_x; fcc: fcc FeH_x; tet: tetragonal FeH_2 type; and cub: cubic FeH_3 type. In the column, the phases observed from low temperatures are shown in parentheses. In run 130, dhcp was observed during decompression after laser heating. $E_{x\text{-}ray}$: energy of x-ray beam.

Run	P (GPa)	T (K)	$\sigma(T)$ (K)	$E_{x\text{-}ray}$ (keV)	Phases	Texture
			FeH_x			
231	26(2)	1690–2179	150	30	fcc, (dhcp)	subliq.
531	26(2)	2601	636	30	fcc, (dhcp)	liq.
103	66(4)	1863–2474	238	37	tet	subliq.
203	89(6)	1888–2692	200	37	tet, cub, (dhcp)	–
			$(Fe_{0.94}Ni_{0.06})H_x$			
131b	33(2)	2499–2791	150	37	dhcp	liq.
231b	33(2)	2508	150	37	dhcp	liq.
331b	33(2)	2639	150	37	dhcp	liq.
431b	33(2)	2748	150	37	dhcp	liq.
130	77(4)	1881–2718	150	37	fcc, tet	liq.

6.5(4) mol % Ni by quenching the FeNi liquid at 1973 K and 1 bar following the method in Nasch *et al.* [14]. The sample was compressed in the diamond-anvil cell (DAC) according to the following process: we drilled the sample chamber in a precompressed rhenium gasket, which we later coated with gold ($\geqslant 80$ Å in thickness) to prevent embrittlement by hydrogen during experiments [7]. Then a foil of sample was loaded into the sample chamber, which was propped on both sides by pieces of the same material to avoid contact with the anvils for better laser heating. We also loaded a piece of ruby [15] and gold [16] for pressure measurements, which were kept apart from the sample to avoid contamination during laser heating. Finally, pure hydrogen gas was loaded into the sample chamber using our gas loading system at Arizona State University.

We measured x-ray diffraction (XRD) patterns at *in situ* high pressure and high temperature in the laser-heated diamond-anvil cell at the 13-IDD beamline of the GSECARS sector of the Advanced Photon Source (Table I for experimental runs). A monochromatic x-ray beam with energy of 30 or 37 keV was coaxially aligned with double-sided near-infrared laser-heating beam. The size of x-ray beam on the sample was 3×4 μm^2 and the size of heated spot was 20 μm in diameter. We used diffraction patterns of a LaB_6 standard to calibrate for the sample-to-detector distance (approximately 200 mm) and correct the tiling of the detector.

Laser heating with pure hydrogen is challenging because high temperatures enhance its already high reactivity and high diffusion at high pressure making the diamond anvil and gaskets brittle, increasing the likelihood for anvil failure. In order to reduce the problem, we coated gaskets with gold [7] and conducted pulsed-laser heating [17].

Pulsed-laser heating was implemented at APS to allow *in situ* XRD measurement at high temperature. In the laser heating system at the beamline, a 1064-nm wavelength infrared laser is focused to a sample in a diamond-anvil cell with a flat-top spot size of around 20 μm in diameter [18,19]. For heating, we accumulated 100 000 laser pulses of 1 μs width at a rate of 10 kHz. The heating time totals to 10 s for the accumulation (including time between pulses) and the sample is estimated to be at high temperature for approximately 0.1 s for the heating spot. We repeated a few shorts in order to make a total heating duration of close to 1 s. The gate of the x-ray detector is synchronized with the pulsed laser beam to accumulate diffraction patterns at high temperatures. For the pulsed laser heating setup combined with gated x-ray diffraction, information is available in [19]. Information on the optical set up of the laser heating system combined with x-ray diffraction is available in [18].

The temperature is calculated by fitting a Planck equation to the thermal radiation spectrum collected on both sides of the DAC [18]. We collected 2D diffraction images using a Pilatus detector. 1D integration from 2D images was conducted using the Dioptas software package [20]. We used the PeakPo software package [21] for peak identification and fitting, and unit-cell fitting for the synthesized phases in the LHDAC.

Hydrogen can easily diffuse into metals, $\sim 10^3$ $\mu m^2/s$ at low P-T [22], and the diffusion would be greater in our experiments as most of the laser heating was performed to temperatures above 2000 K. During gas loading, 1500 bars of hydrogen gas is injected into the sample chamber. The pressure is high enough for hydrogen gas to penetrate along microfractures and grain boundaries in the sample foils which are made by cold compressing powder samples. The grain size of metal powder was $\leqslant 1$ μm. Because hydrogen is expected to surround the grains in this configuration at high pressures, combined with rapid diffusion of hydrogen, our experimental setup is expected to provide sufficient conditions for the sample to fully react with hydrogen.

III. RESULTS

A. X-ray diffraction (XRD) observations

During compression to 26 GPa at 300 K, hcp Fe reacts with hydrogen to form dhcp FeH [Fig. 1(a)]. The observation is consistent with previous studies [2]. Upon heating to 1690 K, a new peak appeared at 1.77 Å, which can be assigned to the 200 line of fcc FeH. Although they could overlap with dhcp peaks, we observed decrease in widths and increase in intensities at the location of the fcc 111 and 220 lines, also supporting the formation of fcc FeH at high temperature. We further heated the sample to higher temperatures: at 1866 and 2179 K, where fcc FeH peaks grew stronger. The large

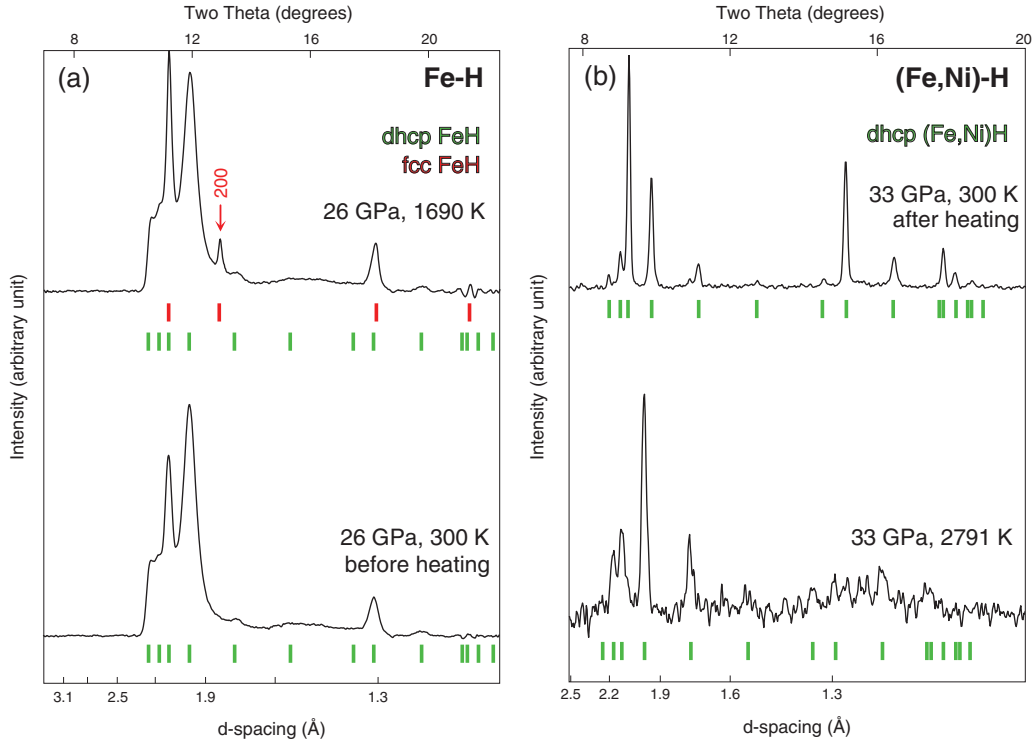

FIG. 1. X-ray diffraction patterns obtained at ∼30 GPa for FeH (a) (x-ray energy was 30 keV; run 231) and FeNiH (b) (x-ray energy was 37 keV; run 131b). The red arrow highlights the 200 peak of fcc FeH. Each heating sequence reads from bottom to top. The green and red ticks show the expected peak positions of the fcc and dhcp phases from their equations of state [7] and crystal symmetry, respectively. dhcp: double hexagonal close-packed structure; fcc: face-centered cubic structure.

unit-cell volume of the synthesized fcc phase (13% larger than that of pure fcc Fe at the same pressure) confirms the significant amount of H present in the phase. We found that molar ratio between Fe and H should be close to 1:1 based on the measured unit-cell volume, which will be discussed in the next section.

At this pressure, peaks from both dhcp and fcc remained in the diffraction patterns during the time of heating and were still present in the temperature-quenched patterns. The system being binary, the coexistence of two phases is thermodynamically possible. Also, it is possible that fcc is the stable phase at high temperatures and dhcp peaks are from the low-temperature regions of the laser heating spot.

We performed a similar experiment for the Ni-bearing system in a H medium at a similar pressure, 33 GPa [Fig. 1(b)]. Similar to the Ni-free system, before laser heating, the $Fe_{1-x}Ni_x$ alloy starting material reacted with hydrogen to form dhcp (Fe,Ni)H at 300 K and high pressures. With heating, dhcp (Fe,Ni)H peaks became sharper, but unlike the Ni-free system, fcc (Fe,Ni)H was not observed up to the highest temperature of the heating cycle 2791 K. Upon quench of the sample to 300 K at high pressures, dhcp (Fe,Ni)H still remained the only phase present in the pattern. Therefore, compared with Ni-free experiments, we found that Ni stabilizes dhcp over fcc at high temperatures and inhibits the formation of fcc despite the low Ni concentration (6.5 mol %) in (Fe,Ni). The same result was reproduced in three other runs at the same pressure and similar temperatures.

Before heating at 66 GPa, the diffraction patterns for pure metallic Fe showed complete reaction with hydrogen to form dhcp FeH [Fig. 2(a)]. During heating at 2145 K, peaks for dhcp FeH were fully replaced by the peaks of tetragonal FeH_2 (space group: $I4/mmm$) indicating a complete transformation of the x-ray probed area. Pépin *et al.* [7] observed the phase at similar pressures, but they heated to lower temperatures ($\leqslant$ 1500 K) and acquired diffraction patterns only after temperature quench. Therefore, our *in situ* diffraction patterns provides direct evidence for the high-temperature stability of tetragonal FeH_2 over 2000 K. We heated the same spot twice more to higher temperatures and confirmed the stability of FeH_2 up to 2474 K (Supplemental Material Fig. 1 [23]).

Unlike the case of the Ni-free sample, we found different phase behaviors in (Fe,Ni)H during heating at 77 GPa [Fig. 2(b)]. At 1881 K, dhcp (Fe,Ni)H is fully replaced by a mixture of fcc (Fe,Ni)H and tetragonal $(Fe,Ni)H_2$. Peaks of fcc (Fe,Ni)H were much more intense than those from $(Fe,Ni)H_2$. At 2718 K, $(Fe,Ni)H_2$ disappeared and only fcc (Fe,Ni)H is present in the pattern. Only fcc was observed in the temperature-quench patterns. At this pressure, the measured volume for fcc (Fe,Ni)H is higher by 15.4% than the volume of Ni-free fcc FeH [24] and +36.1% higher than that of fcc $Fe_{1-x}Ni_x$ with similar Ni contents [25] previously measured at the same pressure (these are reported elsewhere), again confirming the large H solubility in the phases.

In a separate run for Fe metal at 89 GPa and 1888 K, all dhcp FeH transforms into a mixture of FeH_2 and FeH_3 (space group: $Pm\bar{3}m$) [Fig. 3(b)], which both remain in the patterns after temperature quench. This result is consistent with Pépin *et al.* [7] who reported the formation of FeH_3 at 86 GPa. When heating to higher temperatures, FeH_2

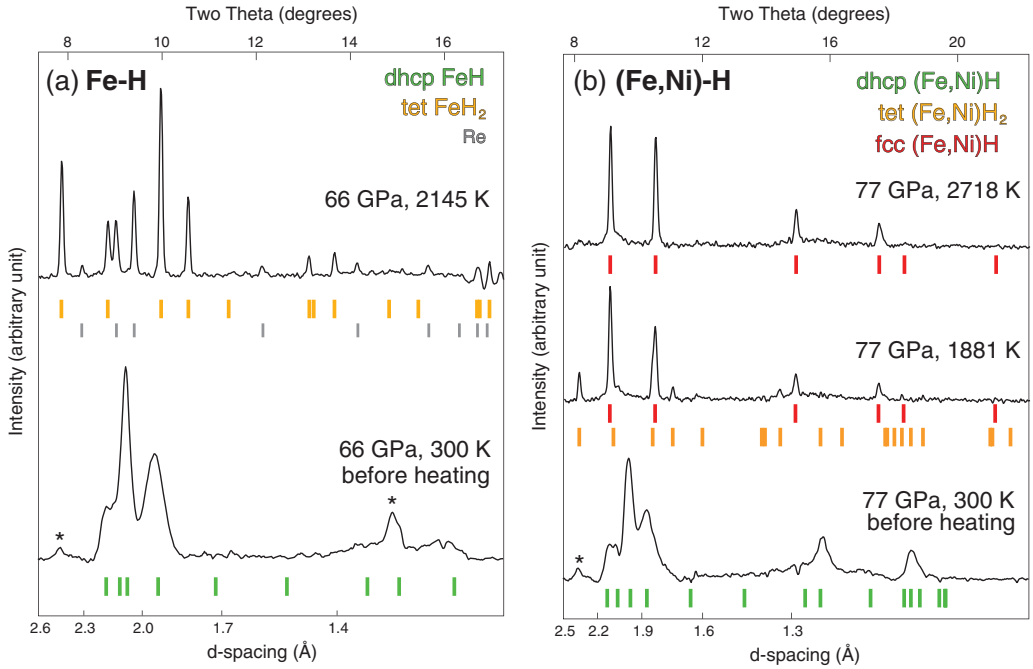

FIG. 2. X-ray diffraction patterns obtained at ∼70 GPa for FeH (a) (run 103) and for FeNiH (b) (run 130). The notations are the same as Fig. 1. Because of the small sample chamber size in LHDAC, some diffraction patterns show peaks from the rhenium gasket. There was no direct contact between the sample and the gasket. dhcp: double hexagonal close-packed structure; fcc: face-centered cubic structure; tet-FeH_2: tetragonal FeH_2 structure [7]. The colored ticks show expected peak positions of different phases from their equations of state [7] and crystal symmetry. These diffraction patterns were measured with a 37 keV x-ray beam.

remains in the patterns but the peak intensity of FeH_3 decreases [Fig. 3(c)]. At 2692 K, diffraction lines of FeH_3 completely disappeared, suggesting possible melting and/or conversion to FeH_2. Note that this is a binary FeH system and therefore partial melting can occur. In the quenched patterns, FeH_3 is absent while FeH_2 is still present. We also found fcc FeH in the quenched patterns, although it was absent at high temperature [Fig. 3(d)]. A reasonable explanation could be that the fcc phase was crystallized from partial melt during temperature quench. The fcc phase also has a much larger unit-cell volume than pure Fe fcc without H. In fact, the phase has a unit-cell volume even greater (by ∼10.5%) than the previously reported volume of FeH at this pressure [24,26] (the unusual volume of the fcc phase is reported elsewhere). Therefore, all the Fe phases observed at this pressure very likely contain large amounts of H.

B. Equations of state (EOS)

Figure 4 shows measured unit-cell volumes of the phases in FeH and FeNiH during decompression. The amount of H can vary in FeH and (Fe,Ni)H alloys: FeH_x and $(Fe,Ni)H_x$. The measured volumes of dhcp FeH are in agreement with previous reports at similar pressures [2,7] as shown in Fig. 4. In these studies, based on the volume expansion expected for an H incorporation [3], $x = 1$ has been inferred. Therefore, we also assume that the dhcp phase has $x = 1$ for H. For the fcc phase, we also found the volume similar or higher than previously reported in the literature [6,24,26] for the ones synthesized below 25 GPa (Fig. 4). The volume is also comparable to the values reported for $x = 1$ fcc FeH_x [6].

We also fitted our measured unit-cell volumes to a Vinet equation [28]. The calculated EOS parameters are included in Table II along with the EOS of related phases from the literature. The measured unit-cell volumes for dhcp (Fe,Ni)H, fcc (Fe,Ni)H, and tetragonal $(Fe,Ni)H_2$ all agree well with EOSs from the literature for corresponding phases in FeH [6,7]. The result is consistent with what is observed for hcp Fe and hcp $Fe_{1-x}Ni_x$ where Ni does not significantly affect the volume of hcp $Fe_{0.8}Ni_{0.2}$ [29] or that of hcp $Fe_{0.9}Ni_{0.1}$ [25] up to Mbar pressures. The agreement in high-pressure volumes results in very little changes in fitted EOS parameters of the phases (Table II). The measured volume for the FeH_2 and FeH_3 phases after temperature quench at high pressure is similar to that observed by Pépin *et al.* [7] at the same conditions.

IV. DISCUSSION

A. Possibility of melting

All *P-T* conditions for our experiments are reported in Fig. 5, along with data from the literature [6,7,26,32–34]. FeH alloys have been shown to have a lower melting temperature (by several hundred kelvins) than pure iron metal below 25 GPa [32,34] (Fig. 5). However, above 25 GPa, the melting behavior is unknown. Furthermore, melting temperatures of polyhydrides (i.e., FeH_x, with $x \geqslant 2$) have not been measured so far to our knowledge.

If the melting curves of FeH and (Fe,Ni)H alloys reported by low-pressure studies are extrapolated to higher pressures, most of our data points would lie above them. However, it is uncertain if the extrapolation would be valid because the

TABLE II. Equation-of-state parameters from experiments. V_0 is the volume, K_0 is the bulk modulus, and K_0' is its pressure derivative at room temperature and 1 bar. For fcc (Fe,Ni)H and tetragonal (Fe,Ni)H_2, we fixed K_0' to the values reported for the FeH phases [6,7,10].

Phase	V_0/Z (Å^3)	K_0 (GPa)	K_0'	Reference
bcc Fe	11.77(7)	162(5)	5.5(8)	Takahashi *et al.* [30]
bcc $Fe_{0.95}Ni_{0.05}$	11.80(7)	155(10)	4.2(8)	Takahashi *et al.* [30]
bcc $Fe_{0.9}Ni_{0.1}$	11.81(7)	155(10)	5.7(8)	Takahashi *et al.* [30]
hcp Fe	11.18(3)	164.8(3.6)	5.33(9)	Mao *et al.* [29]
hcp Fe	11.21(3)	163.4(7.9)	5.38(16)	Dewaele *et al.* [27]
hcp $Fe_{0.8}Ni_{0.2}$	11.19(8)	171.8(2.2)	4.95(9)	Mao *et al.* [29]
hcp $Fe_{0.9}Ni_{0.1}$	11.09(8)	185.1(1.7)	5.31(6)	Sakai *et al.* [25]
fcc Fe	12.26(3)	111.5(1.8)	5.2(2)	Tsujino *et al.* [31]
dhcp FeH	13.9(1)	131.1(3.0)	4.83	Pépin *et al.* [7]
dhcp $(Fe_{0.95}Ni_{0.05})H$	13.8(1)	154.4(3.7)	5	this study
fcc FeH	13.5(1)	99(3)	11.7	Narygina *et al.* [6]
fcc $(Fe_{0.95}Ni_{0.05})H$	13.7(1)	79(4)	11.7	this study
Tetragonal FeH_2	17.0(1)	127.2(8.1)	5	Pépin *et al.* [7]
Tetragonal $(Fe_{0.95}Ni_{0.05})H_2$	17.0(6)	127.8(7.5)	5	this study

solid phases undergo transitions at higher pressures. Such transitions often result in an increase in melting temperature with an increase in dT/dP slope [35]. For the data points near the melting temperatures of H-free Fe metal or FeNi alloy, the samples might have undergone complete melting. The reason is that the system is binary for FeH and ternary for FeNiH. For the same reason, it is possible that most of our data points below the melting curve of pure Fe metal may have undergone partial melting. For example, for FeH at 89 GPa, fcc FeH was not observed during heating up to the highest temperature but was found after temperature quench. Instead, during heating, we observed conversion from $FeH_2 + FeH_3$ to FeH_2 only. It is therefore likely that fcc formed from a partial melt. This observation also suggests that the H content of stable iron hydrides decreases with increasing temperature at a given pressure.

For the heated spots where we achieved temperature near the melting of pure Fe metal (therefore most likely melting for FeH_x) and we found phase behaviors potentially related to the melting (discussed in the paragraph above), we found an eye-shaped structure at the heated spot after laser heating (Fig. 6). For example, all four runs for (Fe,Ni)H at 33 GPa resulted in clear eye-shaped structures: transparent looking center filled with a hydrogen medium surrounded by metal sample. On the other hand, our run for FeH at 66 GPa and measured T up to 2474 K does not display any texture that can be associated with partial melting (or subliquidus). At the center of the eye-shaped structure, we found very weak diffraction lines of FeH_x or (Fe,Ni)H_x phases. For example, the *in situ* diffraction pattern presented in the bottom of Fig. 1(b) shows much more fluctuation in the background. The reason is that the diffraction lines detected have much lower intensities than other diffraction patterns. In fact, the temperature of the heating was above the melting of pure Fe metal and therefore the temperature could have been very close to the liquidus of Fe-H binary.

The eye-shaped structure is likely formed by migration of alloys toward lower temperature regions during melting, leaving the hottest region filled with a hydrogen medium. Note that the eye-shaped structure cannot result from hydrogen melting because hydrogen melts at much lower temperatures (600–1000 K [37]). Additionally, heating at such low temperatures did not result in the eye-shaped structure. For the highest temperature run at 77 GPa for (Fe,Ni)H_x, the temperature was close to the melting temperature expected for H-free $Fe_{0.9}Ni_{0.1}$ [36]. After the heating we found the eye-shaped structure. From these observations, it is feasible that the temperature is above the solidus of FeNiH ternary system.

Anzellini *et al.* [35] used the XRD technique to determine the melting of pure Fe metal in LHDAC. The method involves the detection of diffuse scattering from melt. However, we found that it is very difficult to conduct similar measurements with pulsed laser heating. Once temperature increases above melting, the diffraction from crystalline phases could be reduced. A good example of this can be seen in Fig. 3, where the intensity of FeH_3 peaks diminishes with increasing temperature to completely disappear at 89 GPa and 2692 K. Also, the large signal to noise we found while heating to 2791 K at 33 GPa can result from melting, which could be confirmed by the eye-shaped structure observed after temperature quench. It is therefore likely that many of the phases we observed after temperature quench are crystallization products from melt at high pressures.

B. Effect of Ni on phase stability in FeH

Despite the fact that they are both $3d$ transition metals, alloying behaviors of iron and nickel with hydrogen are quite different. Below 5 GPa at 300 K, iron begins to alloy with H by forming dhcp [2]. However, nickel and hydrogen forms fcc-structured NiH alloys from much lower pressures [3]. With laser heating at pressures above ∼10 GPa, the fcc phase begins to appear in the phase diagrams of both FeH and NiH (Fig. 5). However, their behaviors diverge above ∼50 GPa. At the pressure range, Fe and H begin to form polyhydrides, starting from FeH_2 [7]. However, Ni and H form Ni_2H_3 instead, and a tetragonal-FeH_2 equivalent form is yet to be found experimentally in NiH [8,9].

When alloyed with Fe, Ni has a significant effect on the stable crystal structures of FeH at different P-T, even when

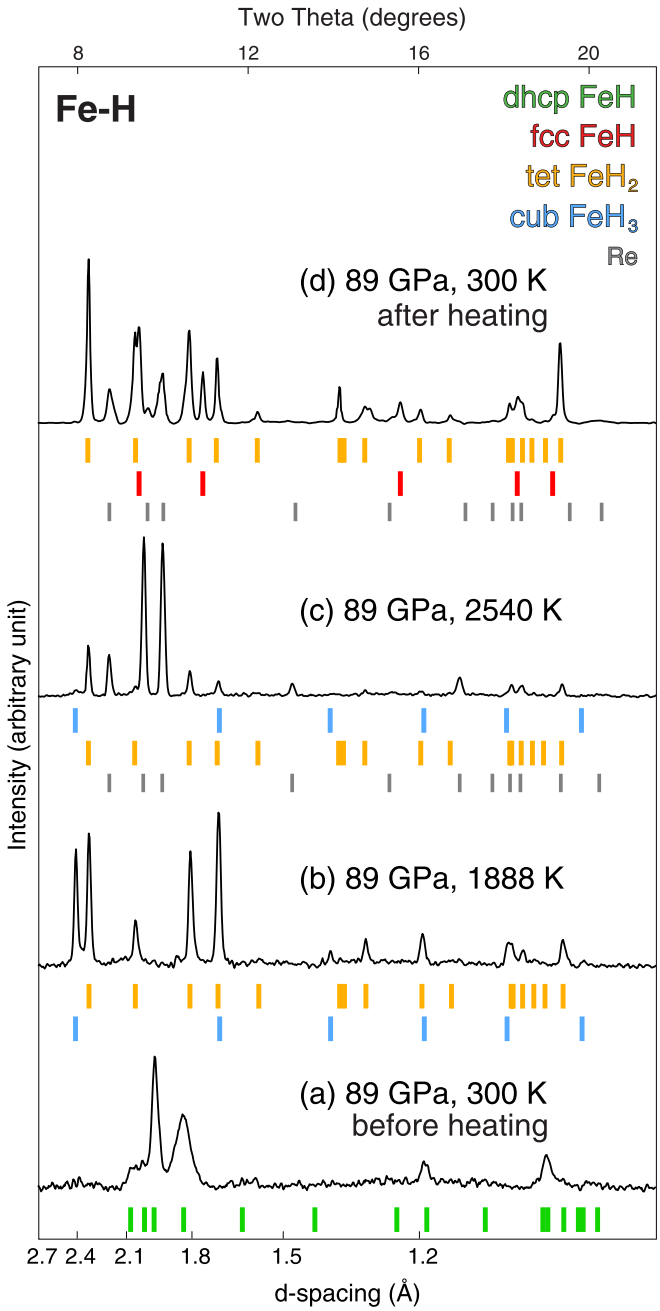

FIG. 3. X-ray diffraction patterns of metallic Fe in H_2 at 89 GPa showing (a) dhcp FeH (green ticks) at 300 K before heating, (b) FeH_2 (orange ticks), and FeH_3 (blue ticks) at 1888 K. (c) As we keep heating at 2539 K, the FeH_3 peaks become weaker. (d) After quench, fcc FeH (red ticks) is present in the pattern. X-ray energy was 37 keV. The diffraction patterns were collected during run 203. Because of the small sample chamber size in LHDAC, some diffraction patterns show peaks from the rhenium gasket. There was no direct contact between the sample and the gasket. dhcp: double hexagonal close-packed structure; fcc: face-centered cubic structure; tet FeH_2: tetragonal FeH_2 structure [7]; cub FeH_3: cubic FeH_3 structure [7]. The colored ticks show expected peak positions of different phases from their equations of state [7,10] and crystal symmetry. Information on the crystal structures of some of these phases are available in [10].

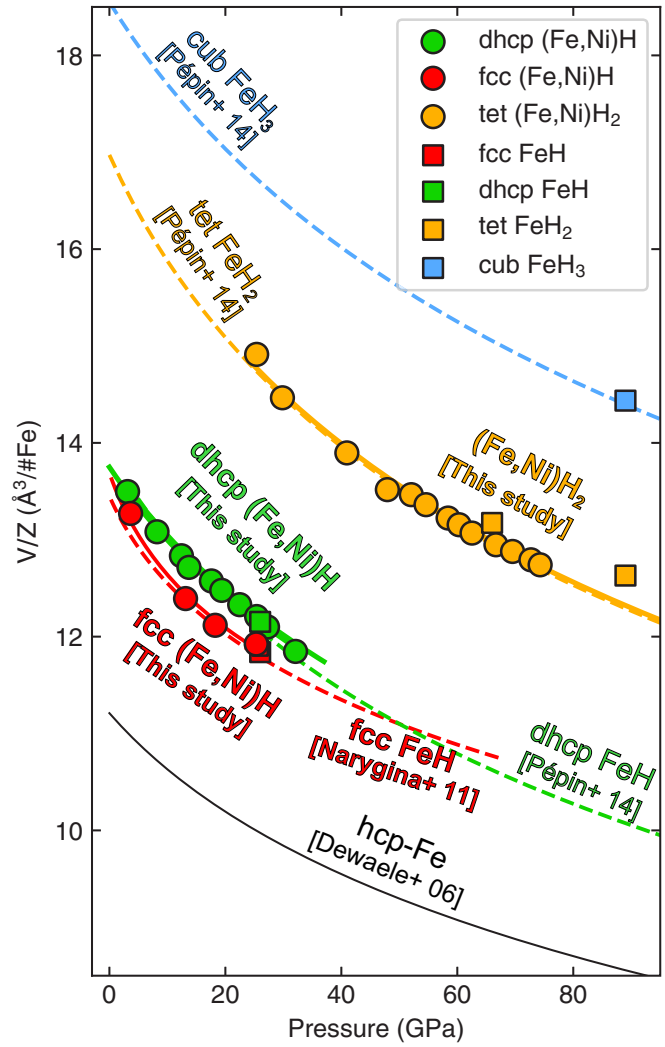

FIG. 4. Pressure-volume relationship of phases in FeNiH (circles) and FeH (squares) at 300 K. The dashed curves represent equations of state from the literature for hcp Fe (black) [27], dhcp FeH (green) [7], fcc FeH (red) [6], tetragonal FeH_2 (yellow) [7], and cubic FeH_3 (blue) [7]. The solid curves represent equations of state from this study for dhcp (Fe,Ni)H (green), fcc (Fe,Ni)H (red), and $(Fe,Ni)H_2$ (yellow). The values used in this table are provided in the Supplemental Material as a table [23].

present in a low amount. We found dhcp phase stable at ~33 GPa and high temperatures in (Fe,Ni)H. In H-free Fe metal, Ni enhances the stability of fcc [38–40]. Furthermore, studies below 20 GPa for (Fe,Ni)H found fcc stability [34]. Even for FeH, both our study and literature data have shown that fcc is stable at high temperatures in this pressure range [Fig. 5(a)]. We believe that all the (Fe,Ni)H data points measured at 33 GPa experienced melting and therefore the dhcp phase is a likely crystallization product from FeNiH melt. However, it is difficult to attribute the unusual stability of dhcp to melting because our fcc observation in FeH at similar pressures was also likely from crystallization from melt. At this time, the origin of the different behavior remains uncertain. If dhcp is indeed more stable in (Fe,Ni)H at ~33 GPa and the multianvil press observation for fcc in (Fe,Ni)H at high

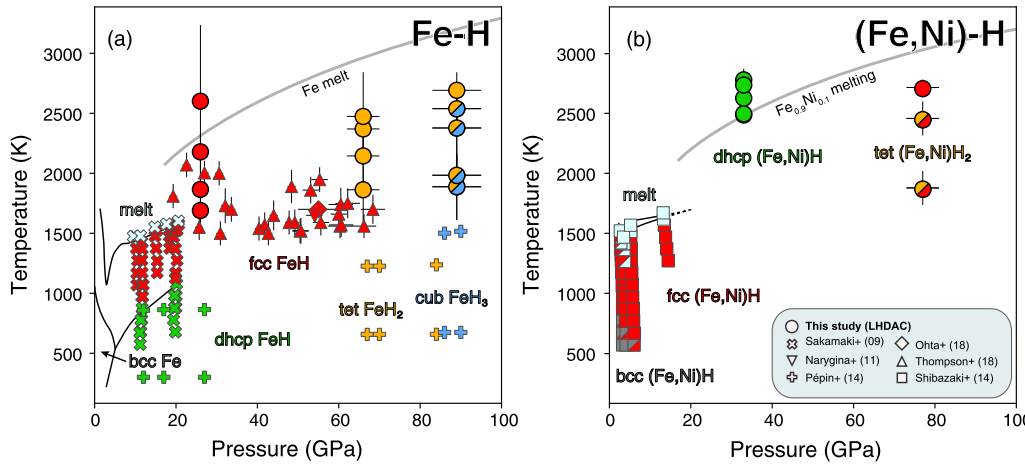

FIG. 5. Pressure-temperature conditions of data obtained for (a) FeH and (b) FeNiH. The colors denote the observed structures: dhcp FeH (green) fcc FeH (red), tetragonal FeH_2 (yellow), and cubic FeH_3 (blue). The phase boundaries and melting curve for FeH below 20 GPa are from a multianvi press study [32]. The melting curve of (Fe,Ni)H below 20 GPa is from a multianvil press study in [34]. Data points from these studies are also presented. Effect of H on the melting temperature is not known above 20 GPa. We presented instead the melting of Fe and FeNi alloy in the figure [35,36]. Diamond-anvil cell data for FeH are included in (a) for comparison [6,7,26,33]. The estimation method for temperature uncertainty can be found in the caption of Table I. bcc: body-centered cubic structure; dhcp: double hexagonal close-packed structure; fcc: face-centered cubic structure; tet FeH_2: tetragonal FeH_2 structure [7]; cub FeH_3: cubic FeH_3 structure [7].

temperature and $P \leqslant 17$ GPa [34] is comparable to our data, the stability of dhcp may be limited to high temperatures.

However, there is an important difference between our study and the multianvil study: the multianvil press study used $LiAlH_4$ as a H source [34]. Shibazaki *et al.* [34] suggested that the absence of dhcp FeH in their experiments could be due to either hydrogen not being supplied to the FeNi sample until the thermal decomposition of $LiAlH_4$ occurring at higher temperature than that of the stability of dhcp (Fe,Ni)H, or that Ni could shift the stability of dhcp (Fe,Ni)H_x to higher pressures with respect to that of dhcp FeH. Since a small amount of Ni seems to change the phase stability of FeH_x, the presence of other elements in Shibazaki *et al.* [34] like Li and Al could cause the observed discrepancy if such elements participate in the reaction in the high-pressure sample chamber.

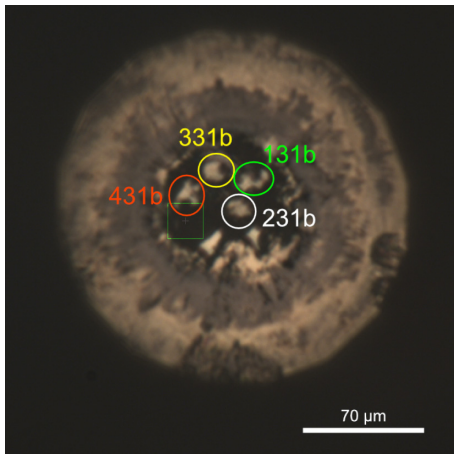

FIG. 6. An optical image showing eye-shaped structures (highlighted by the circles with run numbers) found after laser heating in runs 131b–431b. We interpret that such a structure forms by heating above the liquidus temperature of FeH alloys. The diffraction patterns from the transparent areas at the center of the heating spots show much weaker diffraction peak intensities form metal alloy samples, suggesting that the metal melt may have migrated to colder adjacent areas along the thermal gradients and the transparent areas are filled with hydrogen after melting. The green squared area is an unheated area which can be compared with the heated areas indicated by the colored circles. See Table I for more information on each run.

Nickel also impacts the phase relations in FeH at 77–89 GPa. FeH_2 becomes the dominant phase to the maximum temperatures of heating (2474 K at 66 GPa and 2692 K at 89 GPa) in the Ni-free system. This observation is not only consistent with a previous study [7] but also confirms the stability of the phase to sufficiently higher temperatures relevant for the planetary interiors. With Ni, both fcc and tetragonal-FeH_2 type structures were observed during low-temperature heating. However, fcc was the dominant phase and (Fe,Ni)H_2 ultimately disappears at higher temperatures. Therefore, it appears that Ni increases the pressure at which polyhydride phases appear. We did not observe the monoclinic Ni_2H_3 structure [8,9]. It is perhaps related to the low concentration of Ni in our study.

The stark contrast in phase stability between Ni-free and Ni-bearing FeH phases remains to be explained. One hypothesis could reside in how Ni binds to H with respect to Fe. FeH_x phases for x up to 5 was experimentally observed at 130 GPa [7], and Zhang *et al.* [41] predicted for x up to 6 above 213 GPa. However, NiH_x phases were predicted for only up to $x = 2$ [9,42], which is stable up to at least 300 GPa [42]. Note that in these studies Ni is mainly limiting the stability of polyhydrides. Therefore, it is feasible that Ni may stabilize close-packed structures to higher pressures in Fe-Ni-H.

On a side note, in all of our experiments, hydrogen reacted with $Fe_{1-x}Ni_x$ at room temperature to form dhcp (Fe,Ni)H before heating, which is consistent with the behavior of FeH [2,7]. We attempted to quench (Fe,Ni)H_x to 1 bar, inspired by the fact that NiH can be synthesized at much lower pressures

than FeH [3]. However, fcc (Fe,Ni)H was not stable at 1 bar but transformed to bcc $Fe_{1-x}Ni_x$ with a volume similar to bcc Fe and bcc $Fe_{1-x}Ni_x$ (with up to 10.26 wt % Ni) at atmospheric conditions [30]. Therefore, hydrogen should have escaped from the structure during decompression. Its presence in the crystal structure together with Fe is not sufficient to retain hydrogen at 1 bar at least for the low-Ni system.

V. CONCLUSIONS AND IMPLICATIONS

Our experiments up to 89 GPa on FeH showed that the phase behaviors previously reported for the same system at lower temperatures ($\leqslant$ 1500 K) and at the same pressure range [7,10] remain similar at temperatures above 2000 K. In particular, we found that FeH_2 and FeH_3 are stable at temperatures (>2000 K) relevant for planetary interiors, opening up possibilities for the stability of these phases in the planetary cores containing significant amounts of hydrogen in the deep interiors. To our knowledge, this is the first direct evidence measured at *in situ* high temperatures for the relevance of the polyhydrides to planetary interiors. We found that Ni severely impacts the phase behaviors in FeH: (1) dhcp becomes stable at 33 GPa at temperatures near melting and (2) fcc remains as the dominant phase at 77 GPa. Although tetragonal-FeH_2 structured phases were also observed in Ni-bearing composition, the amount was much smaller than fcc, suggesting that Ni increases the pressure for the stability of polyhydrides. In contrast, according to the comparison of unit-cell volumes between our data on Ni-bearing phases and Ni-free FeH_x phases from literature (Fig. 4), Ni does not change the volume and equation of state of FeH phases at high pressures.

Our experiments show that even a small amount of Ni can affect the phase diagram of FeH without much impact on equation of state. The result may imply that secondary alloying metals could be used for controlling the *P*-*T* stability of polyhydrides. The idea could be useful to further stabilize high-temperature superconductivity of hydrogen rich alloys and compounds at lower pressures.

The lower density of the Earth's core compared with pure metallic Fe or FeNi alloy requires a significant amount of light elements in the region [43]. The martian core appears to have high concentration of light elements as well, according to the recent InSight mission [5]. A wide range of planets have been found outside of the solar system in recent astrophysical surveys and some of these planets have thick hydrogen envelopes [44–46]. Ingassing of hydrogen has been recently suggested for rocky planets and giant exoplanets [47,48]. For the Earth, some recent models have argued for storage of hydrogen in the core [4,49] and strong affinity of hydrogen to metallic iron at high pressures in experiments have supported the argument [2,6]. Models so far have mainly focused on FeH alloy systems for understanding effects of H on planetary cores. Our study highlights the importance of minor alloying elements in the planetary cores, in this case Ni, on the solubility of hydrogen in the region. As shown in our study, Ni may stabilize dense close-packed structures over polyhydrides at least up to approximately 80 GPa, which can impact the amount of hydrogen possibly stored in the planetary cores. In addition, such a minor alloying component, Ni, together with hydrogen can also alter the stable crystal structures in the deep regions. Our experiments here focused on amplifying the effects of hydrogen and therefore used a large amounts of hydrogen for the FeNi alloy system. While the H contents may vary widely in different planets' cores, for the Earth and rocky planets, it would be important to control the amount of hydrogen to lower levels to understand how the concentration of hydrogen can also impact the FeNiH system at high pressures and high temperatures relevant for the planetary interiors.

ACKNOWLEDGMENTS

The work has been supported by the NASA (80NSSC18K0353) and NSF (EAR1921298 and AST2005567). H.P. and S.-H.S. were supported partially by the Keck Foundation (PI: P. Buseck). The results reported herein benefit from collaborations and information exchange within NASA's Nexus for Exoplanet System Science (NExSS) research coordination network sponsored by NASA's Science Mission Directorate. A.V.G.C. gratefully acknowledges ASU's supercomputing resources. B.C. acknowledges the support from NSF (EAR-1555388, EAR-1829273). The synchrotron experiments were conducted at GeoSoilEnviroCARS (University of Chicago, Sector 13), Advanced Photon Source (APS). GeoSoilEnviroCARS is supported by the NSF-Earth Science (EAR-1634415) and DOE-GeoScience (DE-FG02-94ER14466). A.P.S. is supported by DOE-BES under contract DE-AC02-06CH11357.

[1] W. F. McDonough, Compositional model for the Earth's core, Treatise Geochem. **2**, 547 (2003).

[2] J. V. Badding, R. Hemley, and H. Mao, High-pressure chemistry of hydrogen in metals: In situ study of iron hydride, Science **253**, 421 (1991).

[3] V. Antonov, Phase transformations, crystal and magnetic structures of high-pressure hydrides of *d*-metals, J. Alloys Compd. **330**, 110 (2002).

[4] S. Tagawa, N. Sakamoto, K. Hirose, S. Yokoo, J. Hernlund, Y. Ohishi, and H. Yurimoto, Experimental evidence for hydrogen incorporation into Earth's core, Nat. Commun. **12**, 2588 (2021).

[5] S. C. Stähler, A. Khan, W. B. Banerdt, P. Lognonné, D. Giardini, S. Ceylan, M. Drilleau, A. C. Duran, R. F. Garcia, Q. Huang *et al.*, Seismic detection of the martian core, Science **373**, 443 (2021).

[6] O. Narygina, L. S. Dubrovinsky, C. A. McCammon, A. Kurnosov, I. Y. Kantor, V. B. Prakapenka, and N. A. Dubrovinskaia, X-ray diffraction and Mössbauer spectroscopy study of fcc iron hydride FeH at high pressures and implications for the composition of the Earth's core, Earth Planet. Sci. Lett. **307**, 409 (2011).

[7] C. M. Pépin, A. Dewaele, G. Geneste, P. Loubeyre, and M. Mezouar, New Iron Hydrides Under High Pressure, Phys. Rev. Lett. **113**, 265504 (2014).

[8] J. Binns, M.-E. Donnelly, M. Wang, A. Hermann, E. Gregoryanz, P. Dalladay-Simpson, and R. T. Howie, Synthesis

of Ni_2H_3 at high temperatures and pressures, Phys. Rev. B **98**, 140101(R) (2018).

[9] J. Ying, H. Liu, E. Greenberg, V. B. Prakapenka, and V. V. Struzhkin, Synthesis of new nickel hydrides at high pressure, Phys. Rev. Mater. **2**, 085409 (2018).

[10] C. Pépin, G. Geneste, A. Dewaele, M. Mezouar, and P. Loubeyre, Synthesis of FeH_5: A layered structure with atomic hydrogen slabs, Science **357**, 382 (2017).

[11] A. Drozdov, M. Eremets, I. Troyan, V. Ksenofontov, and S. I. Shylin, Conventional superconductivity at 203 kelvin at high pressures in the sulfur hydride system, Nature (London) **525**, 73 (2015).

[12] A. Drozdov, P. Kong, V. Minkov, S. Besedin, M. Kuzovnikov, S. Mozaffari, L. Balicas, F. Balakirev, D. Graf, V. Prakapenka *et al.*, Superconductivity at 250 K in lanthanum hydride under high pressures, Nature (London) **569**, 528 (2019).

[13] C. Heil, G. B. Bachelet, and L. Boeri, Absence of superconductivity in iron polyhydrides at high pressures, Phys. Rev. B **97**, 214510 (2018).

[14] P. M. Nasch, M. Manghnani, and R. Secco, A modified ultrasonic interferometer for sound velocity measurements in molten metals and alloys, Rev. Sci. Instrum. **65**, 682 (1994).

[15] G. Shen, Y. Wang, A. Dewaele, C. Wu, D. E. Fratanduono, J. Eggert, S. Klotz, K. F. Dziubek, P. Loubeyre, O. V. Fat'yanov *et al.*, Toward an international practical pressure scale: A proposal for an IPPS ruby gauge (IPPS-Ruby2020), High Press. Res. **40**, 299 (2020).

[16] Y. Ye, V. Prakapenka, Y. Meng, and S.-H. Shim, Intercomparison of the gold, platinum, and MgO pressure scales up to 140 GPa and 2500 K, J. Geophys. Res.: Solid Earth **122**, 3450 (2017).

[17] S. Deemyad, E. Sterer, C. Barthel, S. Rekhi, J. Tempere, and I. F. Silvera, Pulsed laser heating and temperature determination in a diamond anvil cell, Rev. Sci. Instrum. **76**, 125104 (2005).

[18] V. Prakapenka, A. Kubo, A. Kuznetsov, A. Laskin, O. Shkurikhin, P. Dera, M. Rivers, and S. Sutton, Advanced flat top laser heating system for high pressure research at GSECARS: Application to the melting behavior of germanium, High Press. Res. **28**, 225 (2008).

[19] A. F. Goncharov, V. B. Prakapenka, V. V. Struzhkin, I. Kantor, M. L. Rivers, and D. A. Dalton, X-ray diffraction in the pulsed laser heated diamond anvil cell, Rev. Sci. Instrum. **81**, 113902 (2010).

[20] C. Prescher and V. B. Prakapenka, Dioptas: A program for reduction of two-dimensional x-ray diffraction data and data exploration, High Press. Res. **35**, 223 (2015).

[21] S.-H. Shim, PeakPo - A python software for x-ray diffraction analysis at high pressure and high temperature, Zenodo (2020), doi:10.5281/zenodo.3726423.

[22] G. Zhang, H. Yukawa, N. Watanabe, Y. Saito, H. Fukaya, M. Morinaga, T. Nambu, and Y. Matsumoto, Analysis of hydrogen diffusion coefficient during hydrogen permeation through pure niobium, Int. J. Hydrogen Energy **33**, 4419 (2008).

[23] See Supplemental Material at http://link.aps.org/supplemental/10.1103/PhysRevB.104.224106 for a supplementary table containing measured unit-cell volumes of observed phases at various pressures.

[24] C. Kato, K. Umemoto, K. Ohta, S. Tagawa, K. Hirose, and Y. Ohishi, Stability of fcc phase FeH to 137 GPa, Am. Mineral. **105**, 917 (2020).

[25] T. Sakai, S. Takahashi, N. Nishitani, I. Mashino, E. Ohtani, and N. Hirao, Equation of state of pure iron and $Fe_{0.9}Ni_{0.1}$ alloy up to 3 Mbar, Phys. Earth Planet. Inter. **228**, 114 (2014).

[26] E. Thompson, A. Davis, W. Bi, J. Zhao, E. Alp, D. Zhang, E. Greenberg, V. Prakapenka, and A. Campbell, High-pressure geophysical properties of fcc phase FeH_x, Geochem. Geophys. Geosyst. **19**, 305 (2018).

[27] A. Dewaele, P. Loubeyre, F. Occelli, M. Mezouar, P. I. Dorogokupets, and M. Torrent, Quasihydrostatic Equation of State of Iron above 2 Mbar, Phys. Rev. Lett. **97**, 215504 (2006).

[28] P. Vinet, J. Ferrante, J. H. Rose, and J. R. Smith, Compressibility of solids, J. Geophys. Res.: Solid Earth **92**, 9319 (1987).

[29] H. Mao, Y. Wu, L. Chen, J. Shu, and A. P. Jephcoat, Static compression of iron to 300 GPa and $Fe_{0.8}Ni_{0.2}$ alloy to 260 GPa: Implications for composition of the core, J. Geophys. Res.: Solid Earth **95**, 21737 (1990).

[30] T. Takahashi, W. A. Bassett, and H.-K. Mao, Isothermal compression of the alloys of iron up to 300 kilobars at room temperature: Iron-nickel alloys, J. Geophys. Res. **73**, 4717 (1968).

[31] N. Tsujino, Y. Nishihara, Y. Nakajima, E. Takahashi, K.-i. Funakoshi, and Y. Higo, Equation of state of γ-Fe: Reference density for planetary cores, Earth Planet. Sci. Lett. **375**, 244 (2013).

[32] K. Sakamaki, E. Takahashi, Y. Nakajima, Y. Nishihara, K. Funakoshi, T. Suzuki, and Y. Fukai, Melting phase relation of FeH_x up to 20 GPa: Implication for the temperature of the Earth's core, Phys. Earth Planet. Int. **174**, 192 (2009).

[33] K. Ohta, S. Suehiro, K. Hirose, and Y. Ohishi, Electrical resistivity of fcc phase iron hydrides at high pressures and temperatures, C. R. Geosci. **351**, 147 (2019).

[34] Y. Shibazaki, H. Terasaki, E. Ohtani, R. Tateyama, K. Nishida, K.-i. Funakoshi, and Y. Higo, High-pressure and high-temperature phase diagram for $Fe_{0.9}Ni_{0.1}$-H alloy, Phys. Earth Planet. Int. **228**, 192 (2014).

[35] S. Anzellini, A. Dewaele, M. Mezouar, P. Loubeyre, and G. Morard, Melting of iron at Earth's inner core boundary based on fast x-ray diffraction, Science **340**, 464 (2013).

[36] D. Zhang, J. M. Jackson, J. Zhao, W. Sturhahn, E. E. Alp, M. Y. Hu, T. S. Toellner, C. A. Murphy, and V. B. Prakapenka, Temperature of Earth's core constrained from melting of Fe and $Fe_{0.9}Ni_{0.1}$ at high pressures, Earth Planet. Sci. Lett. **447**, 72 (2016).

[37] S. Deemyad and I. F. Silvera, Melting Line of Hydrogen at High Pressures, Phys. Rev. Lett. **100**, 155701 (2008).

[38] J.-F. Lin, D. L. Heinz, A. J. Campbell, J. M. Devine, W. L. Mao, and G. Shen, Iron-nickel alloy in the Earth's core, Geophys. Res. Lett. **29**, 109 (2002).

[39] W. L. Mao, A. J. Campbell, D. L. Heinz, and G. Shen, Phase relations of Fe–Ni alloys at high pressure and temperature, Phys. Earth Planet. Int. **155**, 146 (2006).

[40] Y. Kuwayama, K. Hirose, N. Sata, and Y. Ohishi, Phase relations of iron and iron–nickel alloys up to 300 GPa: Implications for composition and structure of the Earth's inner core, Earth Planet. Sci. Lett. **273**, 379 (2008).

[41] S. Zhang, J. Lin, Y. Wang, G. Yang, A. Bergara, and Y. Ma, Nonmetallic FeH_6 under high pressure, J. Phys. Chem. C **122**, 12022 (2018).

[42] R. Xi, Y. Jing, J. Li, Y. Deng, X. Cao, and G. Yang, New nickel hydrides under high pressure, J. Phys. Chem. C **123**, 24243 (2019).

[43] K. Hirose, S. Labrosse, and J. Hernlund, Composition and state of the core, Annu. Rev. Earth Planet Sci. **41**, 657 (2013).

[44] D. Jontof-Hutter, The compositional diversity of low-mass exoplanets, Annu. Rev. Earth Planet Sci. **47**, 141 (2019).

[45] W. Zhu and S. Dong, Exoplanet statistics and theoretical implications, Annu. Rev. Astron. Astrophys. **59**, 291 (2021).

[46] J. L. Bean, S. N. Raymond, and J. E. Owen, The nature and origins of sub-Neptune size planets, J. Geophys. Res.: Planets **126**, e2020JE006639 (2021).

[47] P. Olson and Z. D. Sharp, Hydrogen and helium ingassing during terrestrial planet accretion, Earth Planet. Sci. Lett. **498**, 418 (2018).

[48] E. S. Kite, B. Fegley Jr, L. Schaefer, and E. B. Ford, Superabundance of exoplanet sub-neptunes explained by fugacity crisis, Astrophys. J. Lett. **887**, L33 (2019).

[49] J. Wu, S. J. Desch, L. Schaefer, L. T. Elkins-Tanton, K. Pahlevan, and P. R. Buseck, Origin of Earth's water: Chondritic inheritance plus nebular ingassing and storage of hydrogen in the core, J. Geophys. Res.: Planets **123**, 2691 (2018).